

Supporting Information

Graphene quantum dots engineered ultrathin loose polyamide nanofilms for high-performance nanofiltration

Yafei Li,^{ab} Xinda You,^{ab} Ya Li,^{ab} Jinqiu Yuan,^{ab} Jianliang Shen,^{ab} Runnan Zhang,^{ab}
Hong Wu,^{abc} Yanlei Su^{*ab} and Zhongyi Jiang^{*abd}

*^aKey Laboratory for Green Chemical Technology, School of Chemical Engineering
and Technology, Tianjin University, Tianjin 300072, China.*

*^bCollaborative Innovation Center of Chemical Science and Engineering (Tianjin),
Tianjin 300072, China.*

*^cTianjin Key Laboratory of Membrane Science and Desalination Technology, Tianjin
University, Tianjin 300072, China.*

*^dJoint School of National University of Singapore and Tianjin University,
International Campus of Tianjin University, Binhai New City Fuzhou, 350207, China.*

** E-mail: suyanlei@tju.edu.cn; zhyjiang@tju.edu.cn*

Experimental section

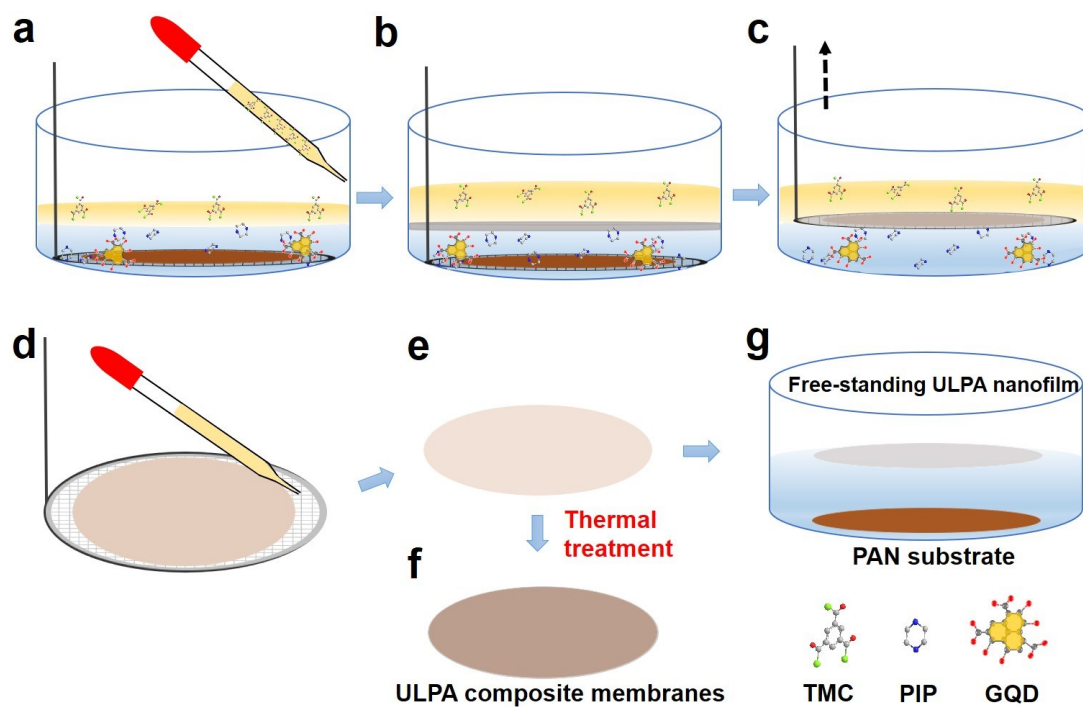


Fig. S1. Schematic illustration of the free-standing ULPA nanofilms prepared at a free aqueous-organic interface. a) PAN substrates were fixed on the mesh and pre-sank on the bottom of aqueous solution containing GQDs and PIP, then addition of the n-heptane containing TMC using a pipette. b) Instantaneous formation of ULPA nanofilms at the free aqueous-organic interface. c) PAN substrates were picked-up by a mesh and ULPA nanofilms were deposited and adhered on them to form composite membranes. d) Rinsing composite membranes with excess n-heptane. e) ULPA nanofilms adhered weakly onto PAN substrates f) The composite membranes underwent thermal treatment at 60 °C for 10 min and ULPA nanofilms adhered tightly onto PAN substrates. g) ULPA nanofilms were floated off the PAN substrates onto water surface.

Table S1. Preparation conditions of different free-standing ULPA nanofilms.

Nanofilm	PIP (g L ⁻¹)	TMC (g L ⁻¹)	GQDs (g L ⁻¹)	Status	t (s)*
PA	0.125	0.100	0.000	--	60
ULPA-1	0.125	0.100	0.025	GQDs	60
ULPA-2	0.125	0.100	0.050	GQDs	60
ULPA-3	0.125	0.100	0.075	GQDs	60
ULPA-4	0.125	0.100	0.100	GQDs	60
ULPA-5	0.125	0.100	0.050	LGQDs-17	60
ULPA-6	0.125	0.100	0.050	LGQDs-45	60
ULPA-7	0.125	0.100	0.050	LGQDs-110	60
ULPA-8	0.125	0.100	0.050	RGQDs-0.61	60
ULPA-9	0.125	0.100	0.050	RGQDs-0.60	60
ULPA-10	0.125	0.100	0.050	RGQDs-0.58	60

* Interface polymerization time.

Results and discussion section

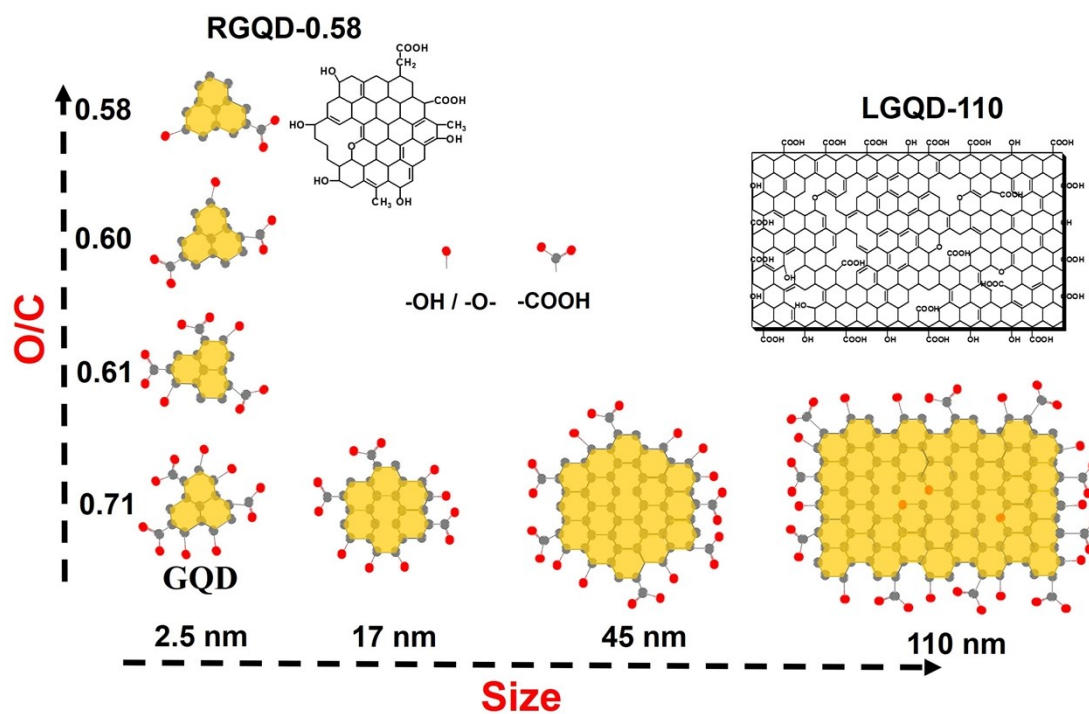


Fig. S2. Chemical structure and schematic diagram of GQDs with different physical size and O/C ratio. The data is obtained from Fig. 1a to 1d in the text and Fig. S4 to S7 in supporting information.

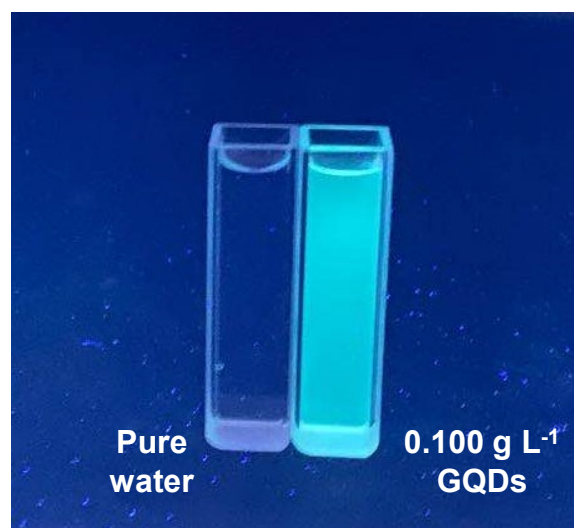


Fig. S3. Fluorescence photograph of pure water and 0.100 g L^{-1} GQDs aqueous solution under 365 nm ultraviolet irradiation.

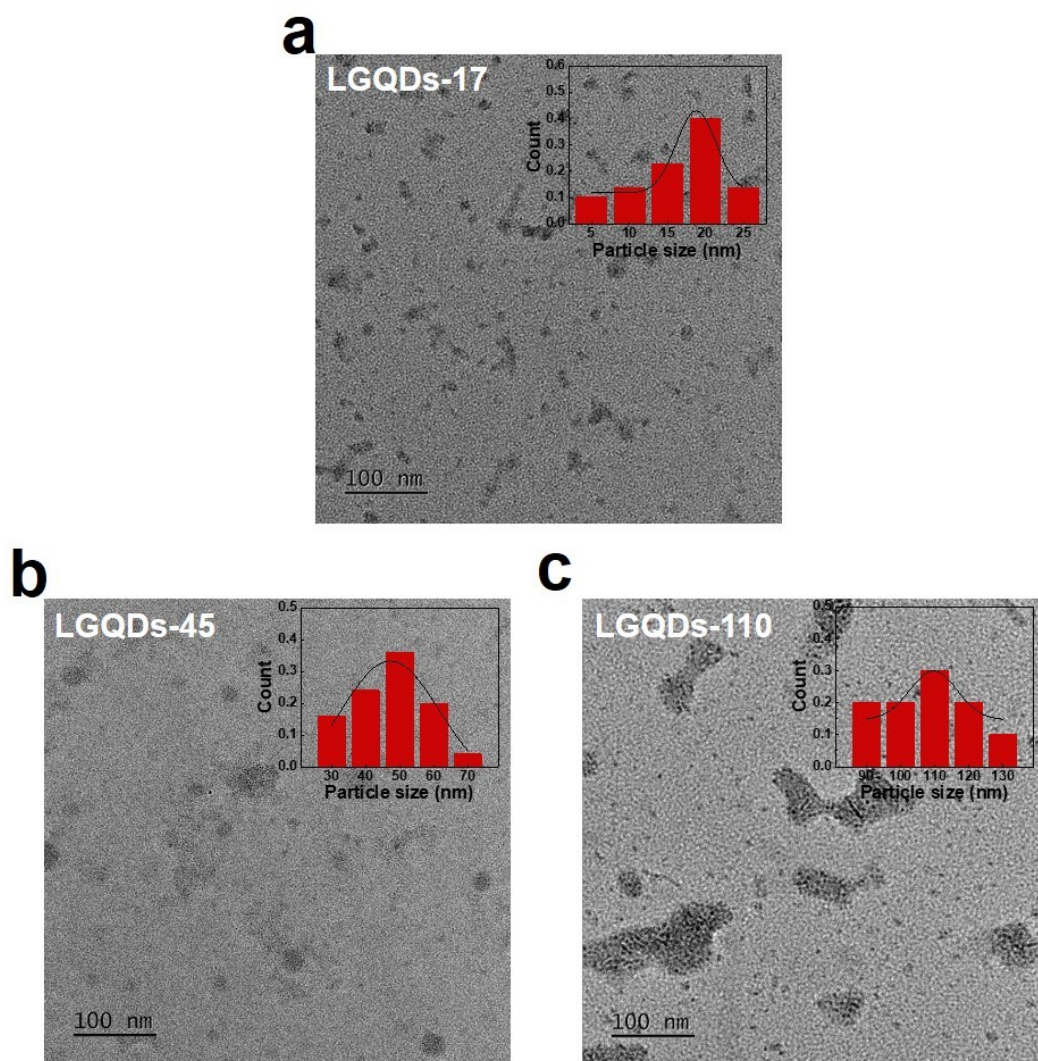


Fig. S4. TEM images of LGQDs. The inset in every image is the size distribution statistics chart. The average sizes of LGQDs in a), b) and d) are 17 nm, 45 nm and 110 nm, respectively.

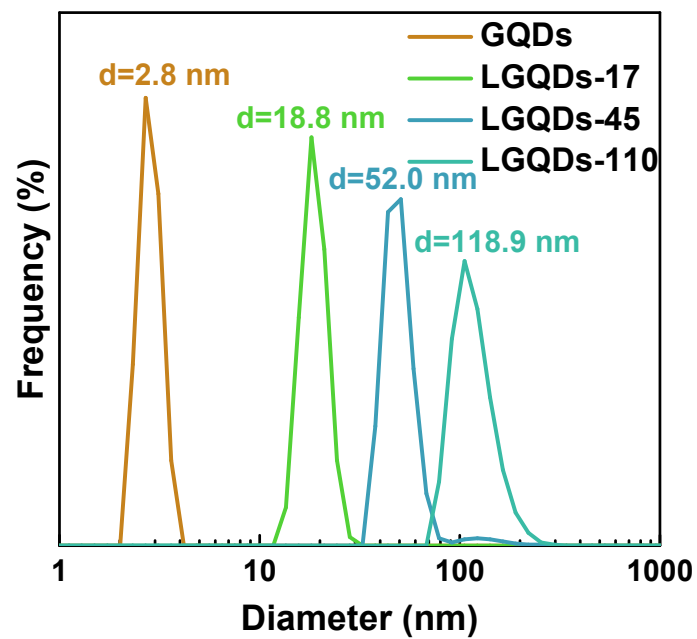


Fig. S5. Size distribution of LGQDs, which were measured by a nanoparticle size analyzer.

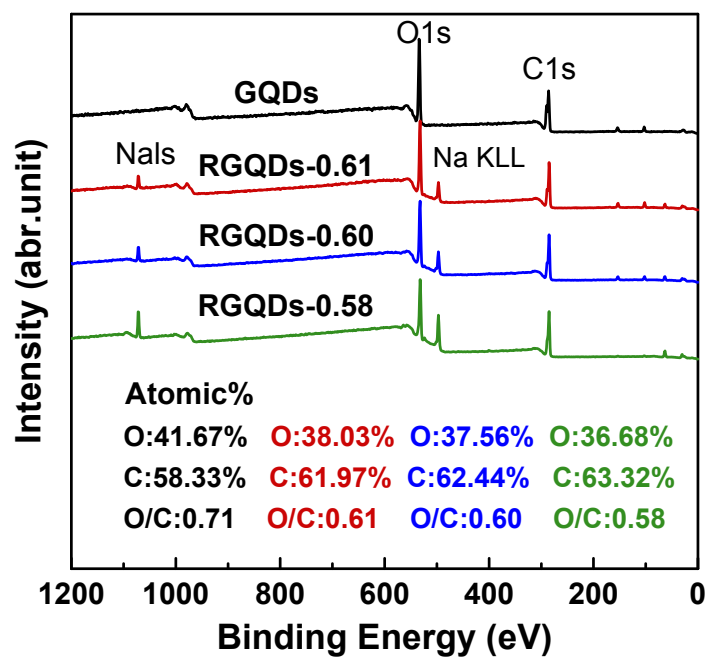


Fig. S6. XPS spectra and the corresponding elemental composition of RGQDs.

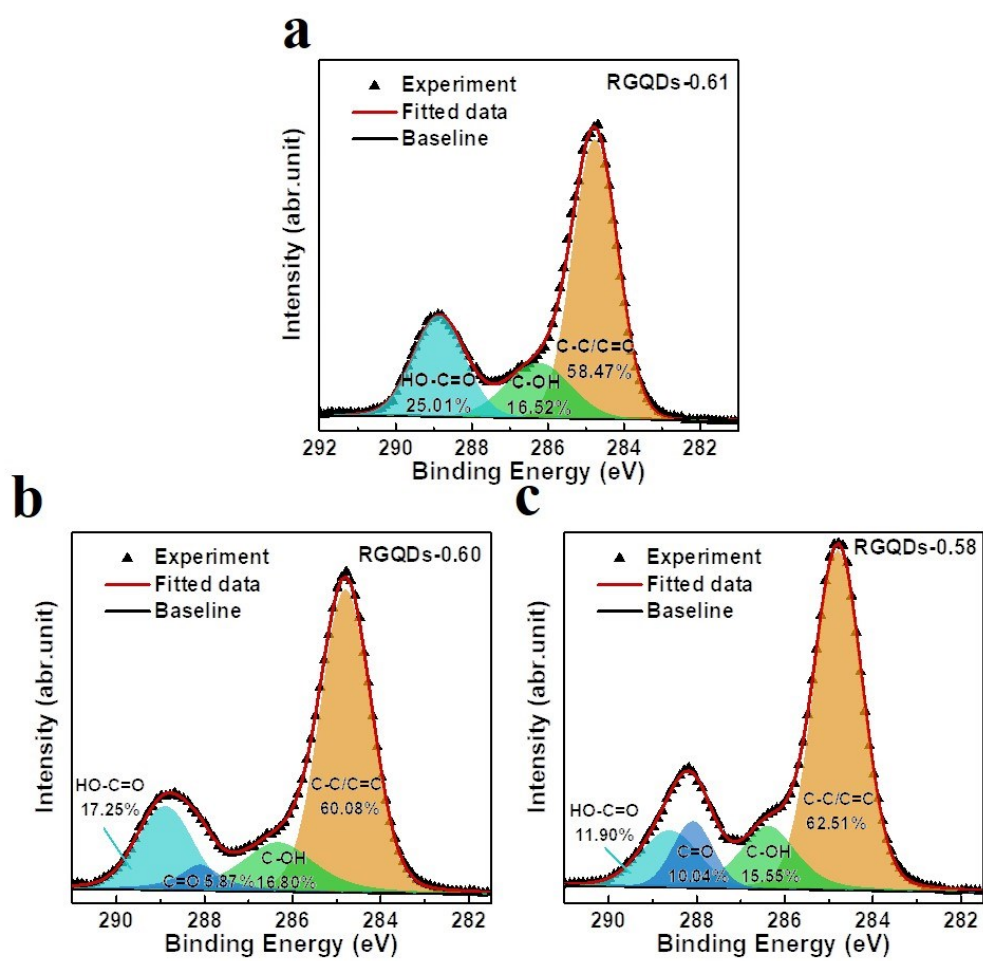


Fig. S7. High-resolution XPS C1s spectra of RGQDs.

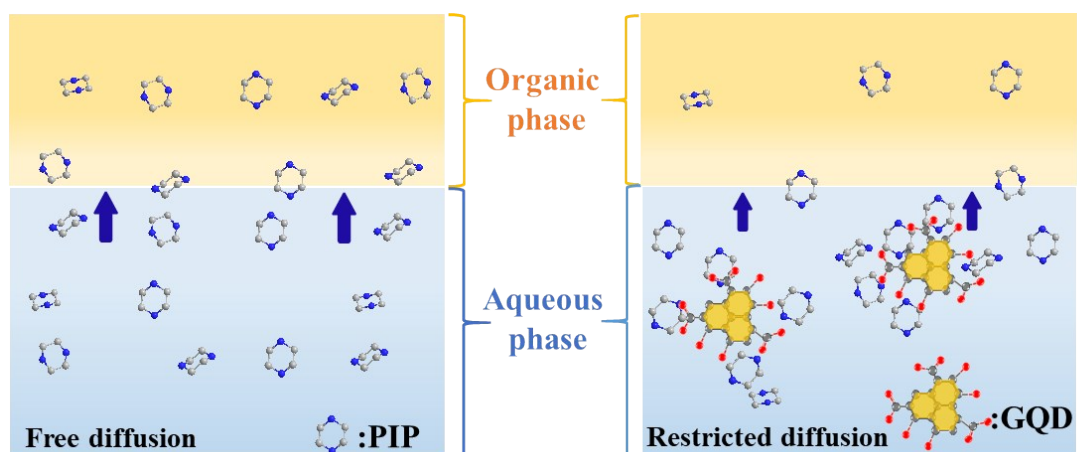


Fig. S8. The influence of GQDs on PIP diffusion. Compared with relatively rapid free diffusion of PIP, when GQDs were added to the aqueous phase, they interacted with PIP through chemical affinity and steric hindrance, resulting in a restricted diffusion.

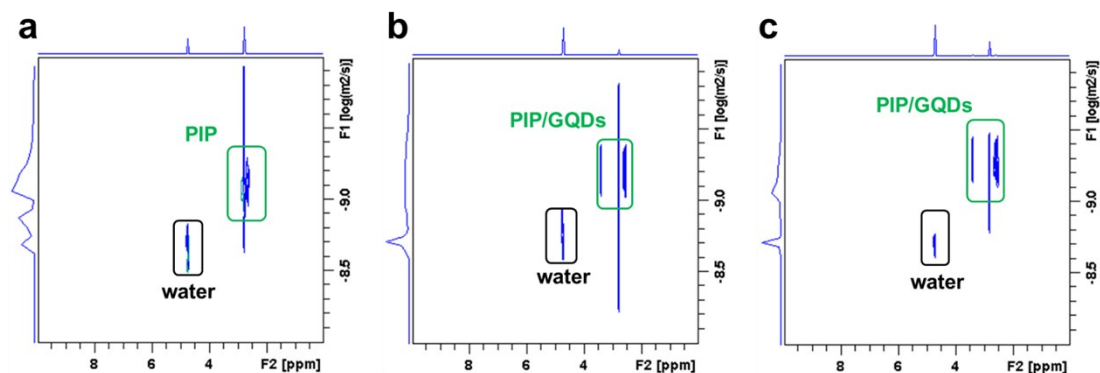


Fig. S9. 2D DOSY NMR spectrum of water and PIP in GQD solution. a) in D_2O ; b) in 0.050 g L^{-1} GQD solution; c) in 0.100 g L^{-1} GQD solution. The diffusion coefficients of PIP in a, b, and c are 6.57×10^{-6} , 6.39×10^{-6} and $6.26 \times 10^{-6} \text{ cm}^2 \text{ s}^{-1}$, respectively, which shows a decrease trend with increasing GQD concentration.

Sample measurement and data analysis: GQDs and PIP were dispersed in D_2O and the concentration of PIP and GQDs was the same as those for nanofilm fabrication. Then, the mixture solution was transferred directly into NMR tubes for measuring the diffusion coefficients of PIP using 2D DOSY NMR. The DOSY spectrum was recorded on a Bruker Avance III 600 spectrometer (Switzerland). All measurements were performed at $25 \text{ }^\circ\text{C}$. The diffusion coefficient of PIP can be calculated from 2D DOSY NMR spectrum. The values of diffusion coefficients were considered by taking centroid of the peak in the DOSY spectrum. Taking Fig. S9b as an example, the centroid of the peak is $10^{-9.19} \text{ m}^2/\text{s}$, which is equal to $6.39 \times 10^{-10} \text{ m}^2/\text{s}$. Thereafter, by unit conversion, we can obtain the diffusion coefficient of ULPA-2 as $6.39 \times 10^{-6} \text{ cm}^2/\text{s}$.

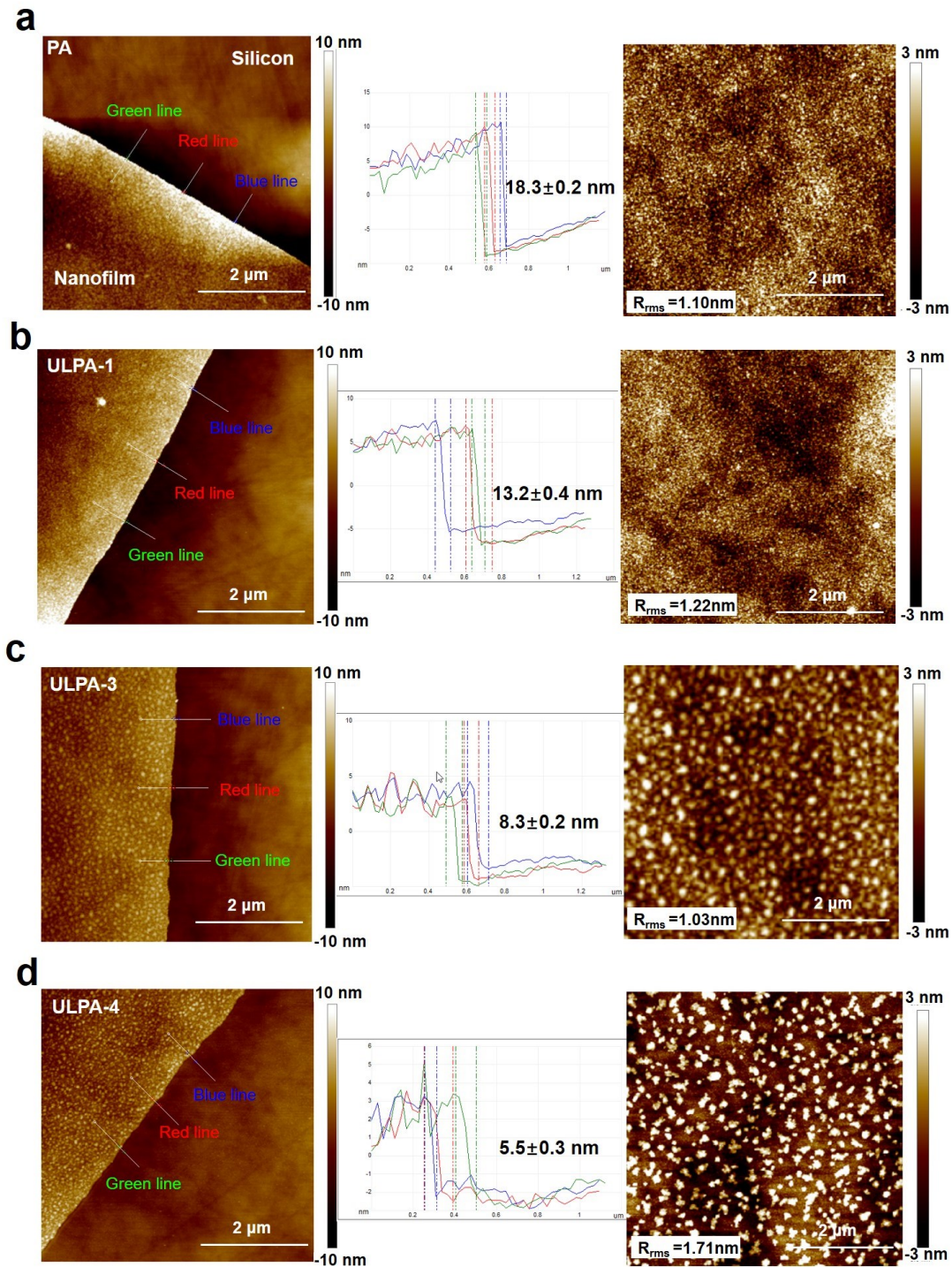


Fig. S10. AFM height images, profiles and topography images of the free-standing ULPA nanofilms transferred onto silicon wafers. a) PA nanofilm; b) ULPA-1 nanofilm; c) ULPA-3 nanofilm; d) ULPA-4 nanofilm. A scratch was made to expose the silicon wafer surface for the measurement of ULPA nanofilm thickness.

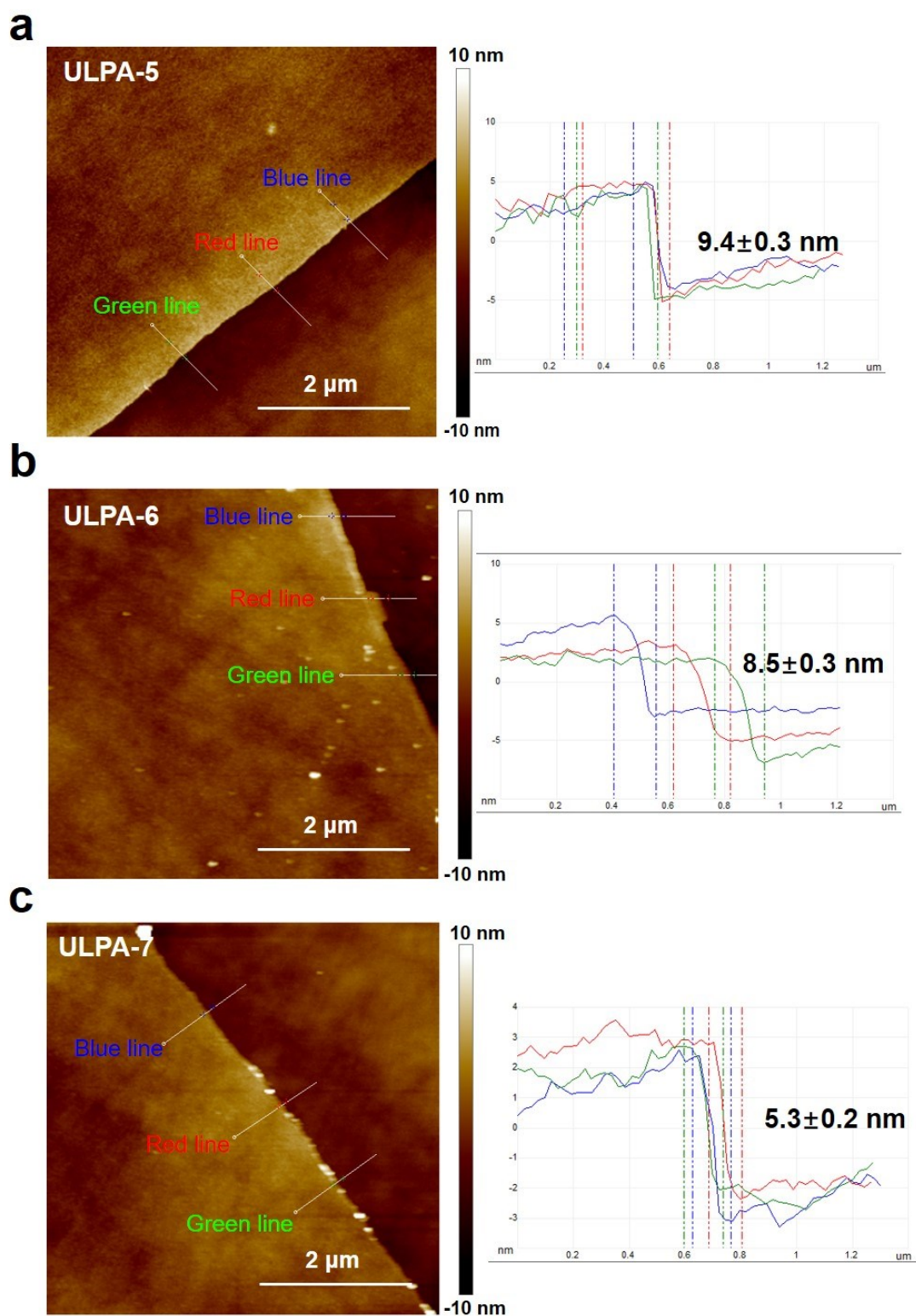


Fig. S11. AFM height images and profiles of the free-standing ULPA nanofilms transferred onto silicon wafers. a) ULPA-5 nanofilm; b) ULPA-6 nanofilm; c) ULPA-7 nanofilm.

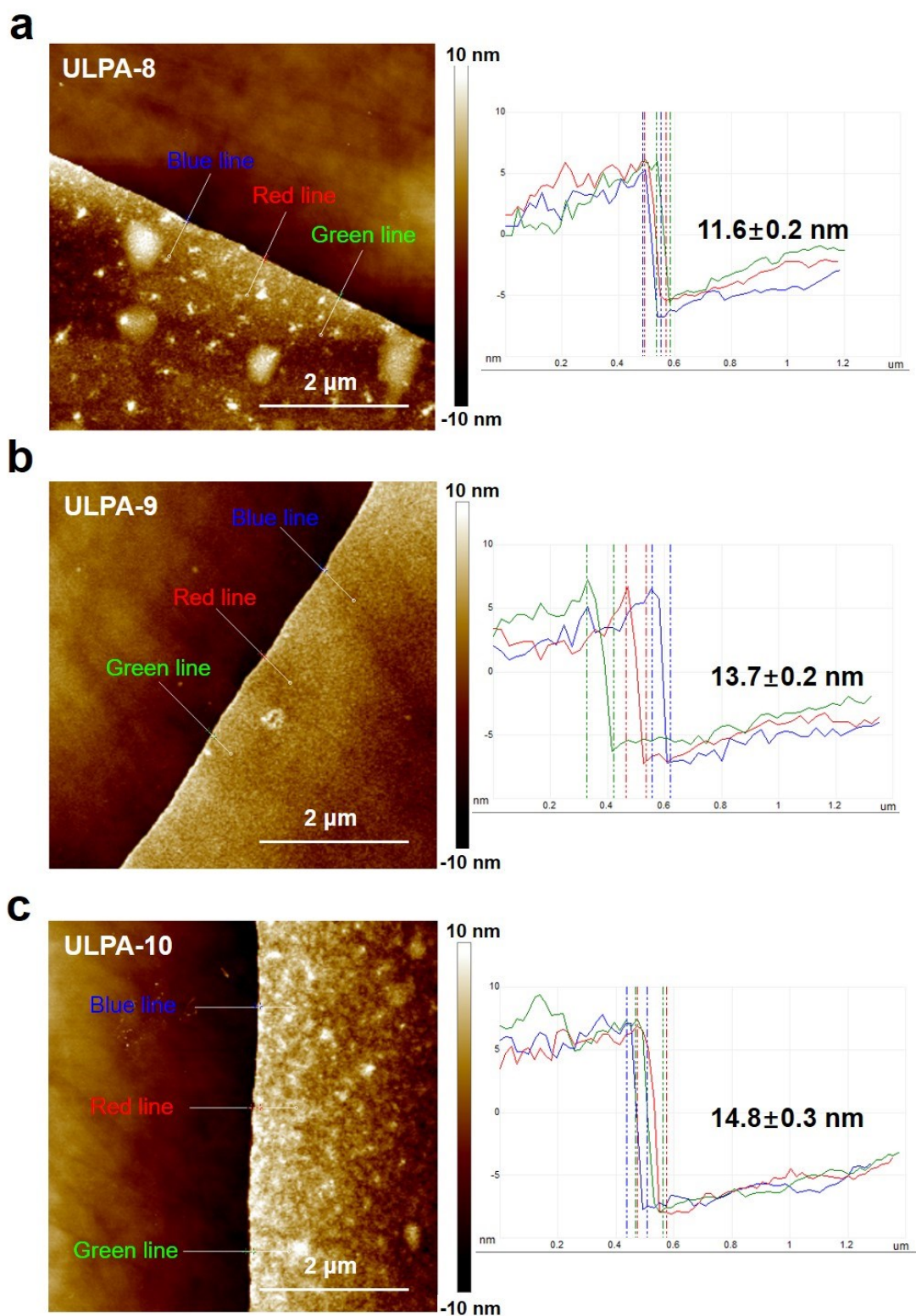


Fig. S12. AFM height images and profiles of the free-standing ULPA nanofilms transferred onto silicon wafers. a) ULPA-8 nanofilm; b) ULPA-9 nanofilm; c) ULPA-10 nanofilm.

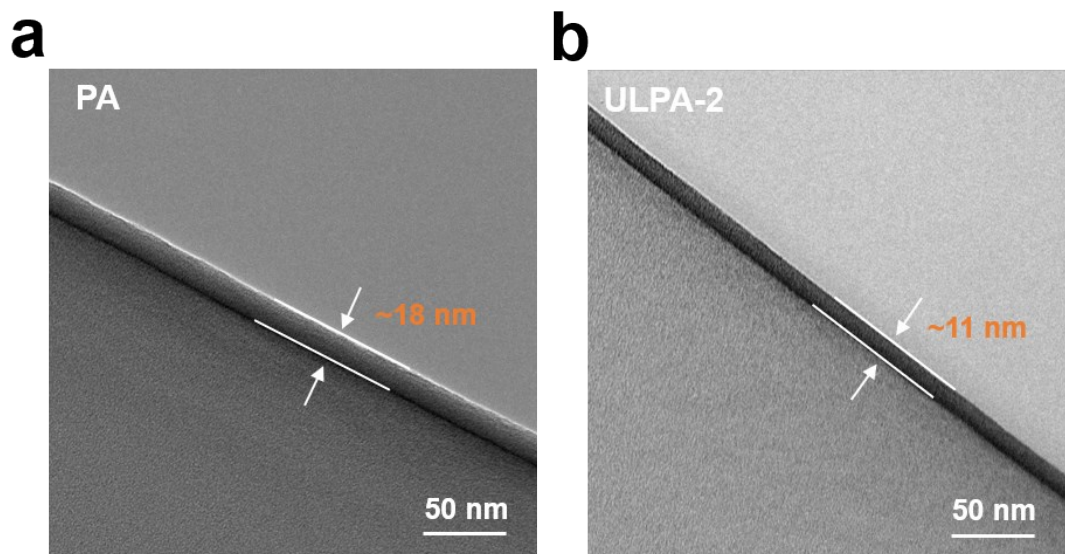


Fig. S13. Cross-sectional TEM images of the PA and the ULPA-2 nanofilms on PAN substrates.

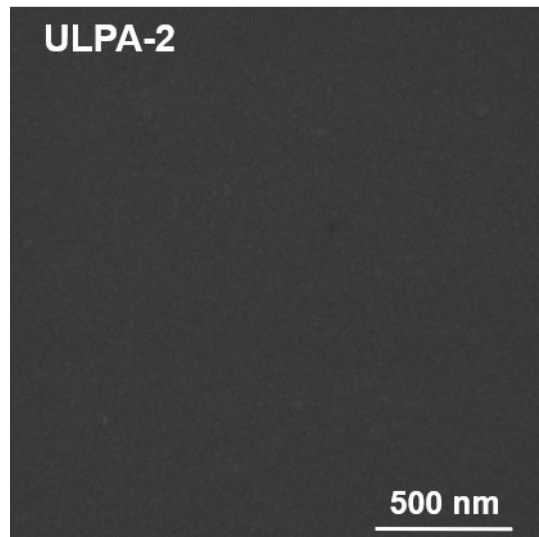


Fig. S14. SEM image of the ULPA-2 nanofilm transferred onto silicon wafer. The ULPA-2 nanofilm was smooth and defect-free. No damage was found after transferring from free aqueous-organic interface onto silicon wafer.

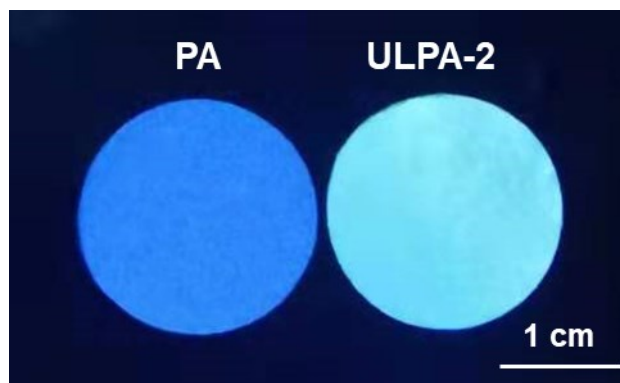


Fig. S15. Fluorescent photograph of the PA and the ULPA-2 composite membranes under 365 nm ultraviolet irradiation.

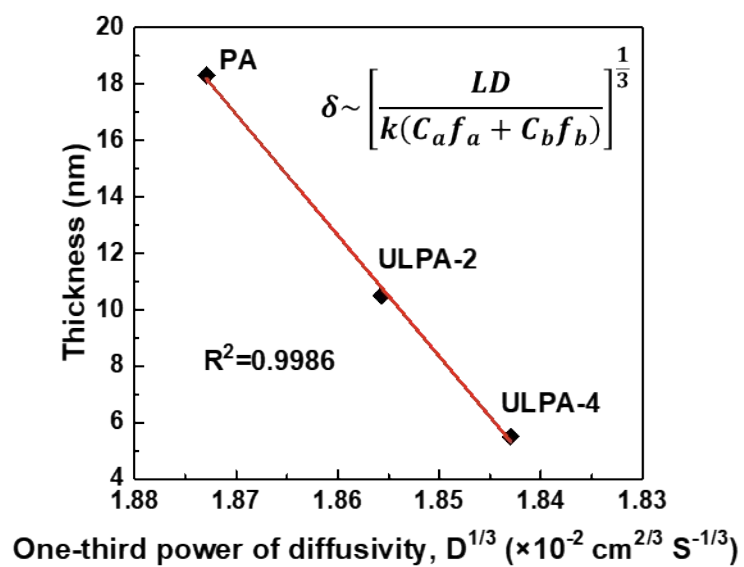


Fig. S16. Correlating one-third power of diffusivity and nanofilm thickness.

We have correlated the one-third power of PIP diffusivity ($D^{1/3}$) and nanofilm thickness (δ). The results showed the same trend as those from the Freger equation and R^2 reached 0.9986, revealing a desirable linear relationship.

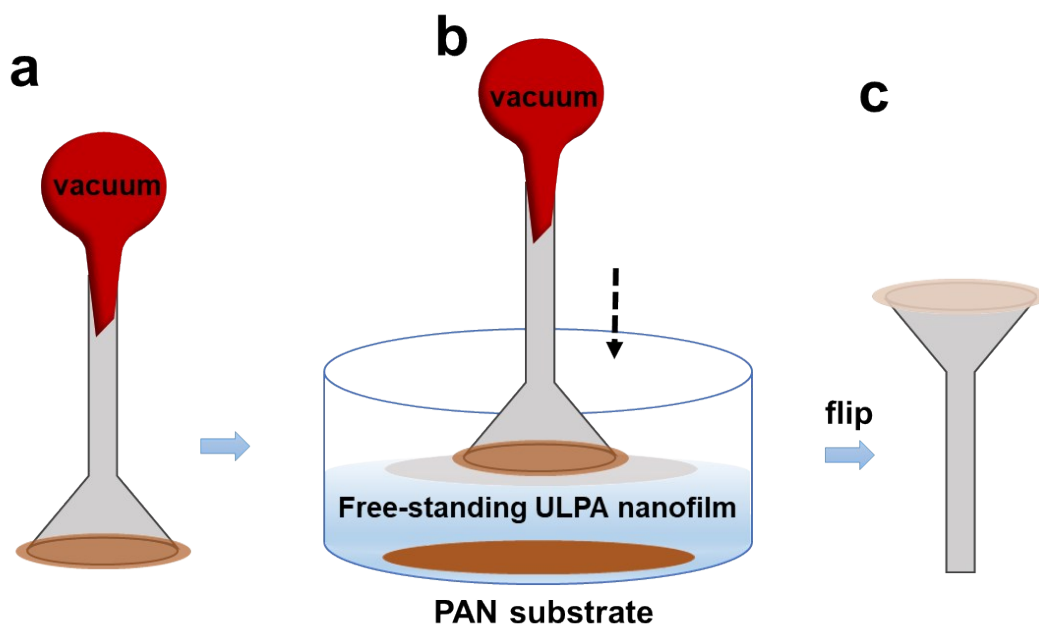


Fig. S17. a) Simple vacuum device, b) The free-standing ULPA nanofilm was drawn under vacuum from the water surface c) Flipped ULPA nanofilm.

In order to flip the free-standing ULPA nanofilms, we made a simple vacuum device using funnel and rubber pipette bulb. The vacuum condition was provided by the rubber pipette bulb. Then, the free-standing ULPA nanofilms were drawn under vacuum from the water surface and flipped. The rear surfaces of the ULPA nanofilms were thus facing up. Thereafter, we could use analytical instruments to confirm their chemical structure of rear surfaces.

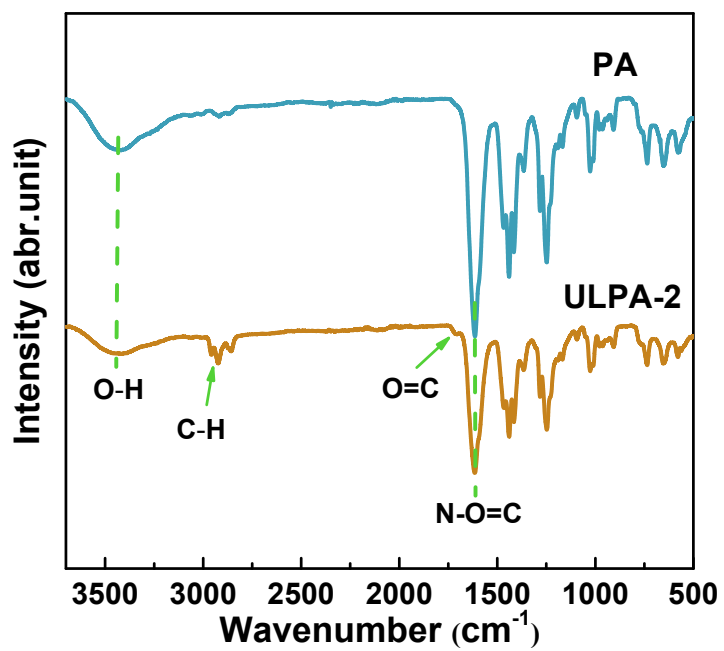


Fig. S18. FTIR spectra of the free-standing ULPA nanofilms. The appearance of peak at 1708 cm^{-1} means the formation of carbonyl group (O=C) of ester bonds.

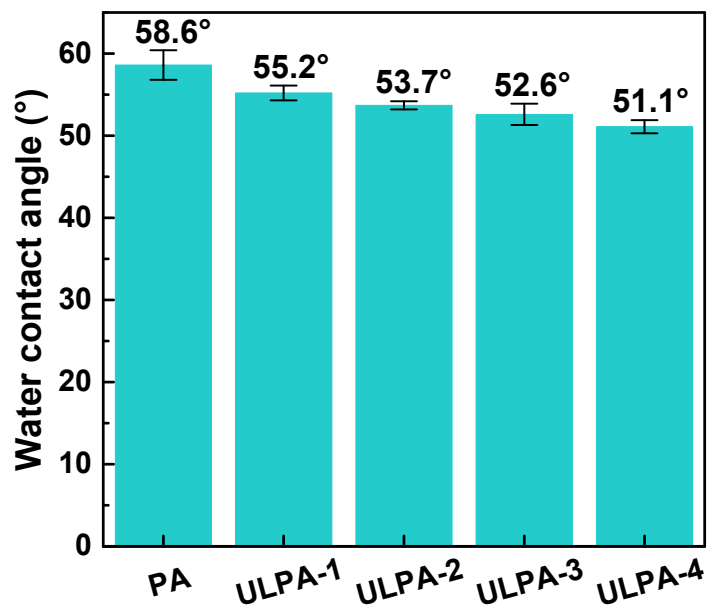


Fig. S19. Water contact angle of the ULPA composite membranes.

Table S2. The elemental compositions and crosslinking degrees (D, %) of front and rear surfaces of the PA and the ULPA-2 nanofilm.

Nanofilm	C (%)	O (%)	N (%)	O/N* ^a	D (%) ^{*b}
PA front	77.2	11.9	10.9	1.09	87.1
PA rear	78.1	11.4	10.5	1.09	87.1
ULPA-2 front	76.9	12.2	10.9	1.12	83.0
ULPA-2 rear	79.2	11.7	9.1	1.29	62.0

^a Element overall atomic ratio obtained directly.

^b The crosslinking degree (D, %) is calculated based on the O/N* ratio using eqn S1 and S2.

$$\frac{O}{N} = \frac{3m+4n}{3m+2n} \quad (S1)$$

$$D = \frac{m}{m+n} \times 100\% \quad (S2)$$

where m and n are the crosslinked and linear proportion of the polyamide nanofilms, respectively.¹

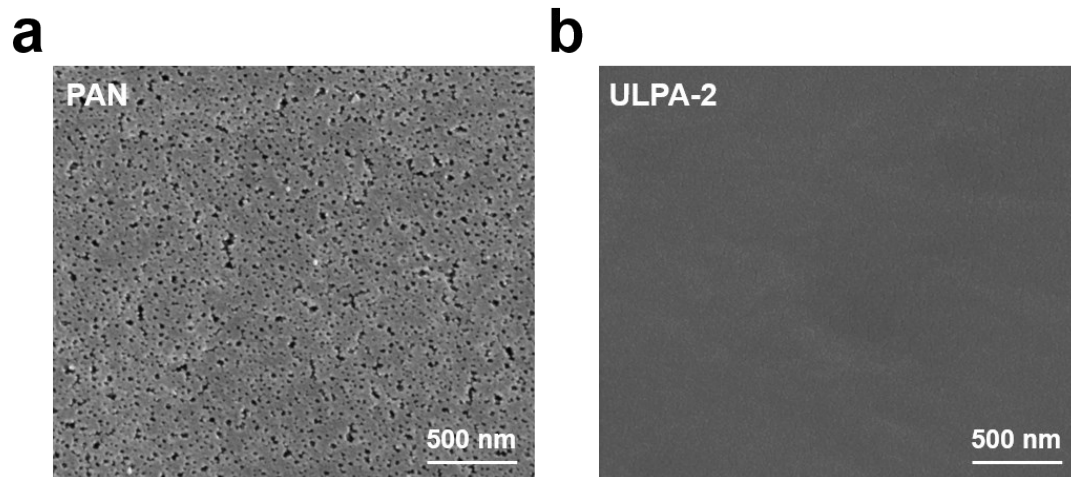


Fig. S20. SEM images of PAN substrate (a) and ULPA-2 composite membranes (b). The free-standing ULPA-2 nanofilm was transferred onto PAN substrate to cover its visible pores.

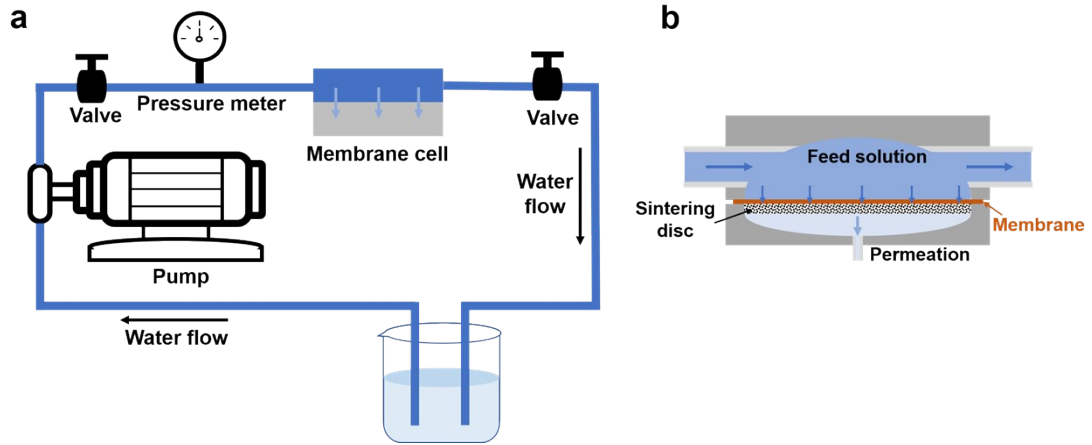


Fig. S21. Schematic illustration of the cross-flow filtration apparatus (a) and section diagram of membrane cell (b).

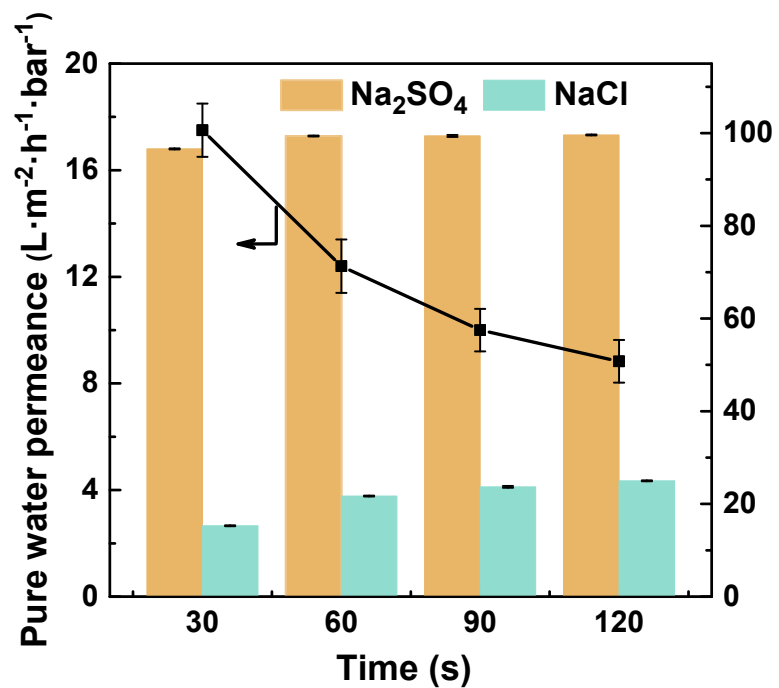


Fig. S22. Separation performance of the polyamide composite membranes prepared in different reaction time. The polyamide nanofilms were prepared from 0.125g L⁻¹ PIP and 0.100 g L⁻¹ TMC at free aqueous-organic interface in different reaction time.

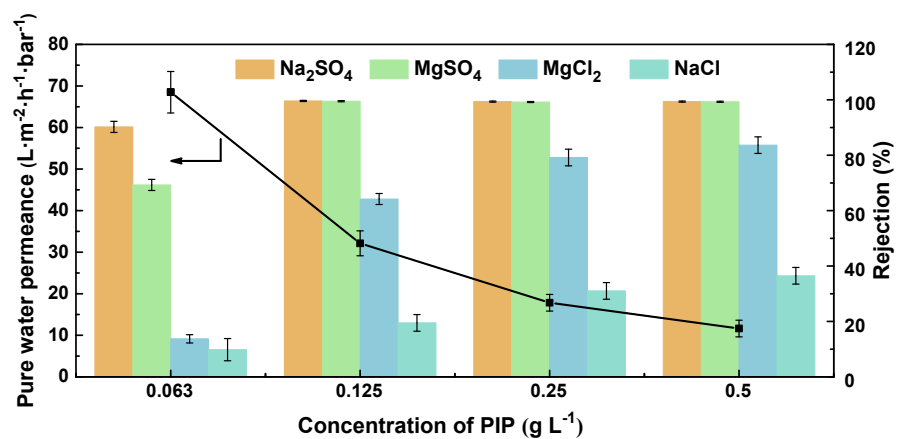


Fig. S23. Separation performance of the ULPA composite membranes prepared with different PIP concentrations. The ULPA nanofilms were prepared from 0.100 g L⁻¹ TMC and 0.050 g L⁻¹ GQDs at free aqueous-organic interface for 60 s with different PIP concentrations.

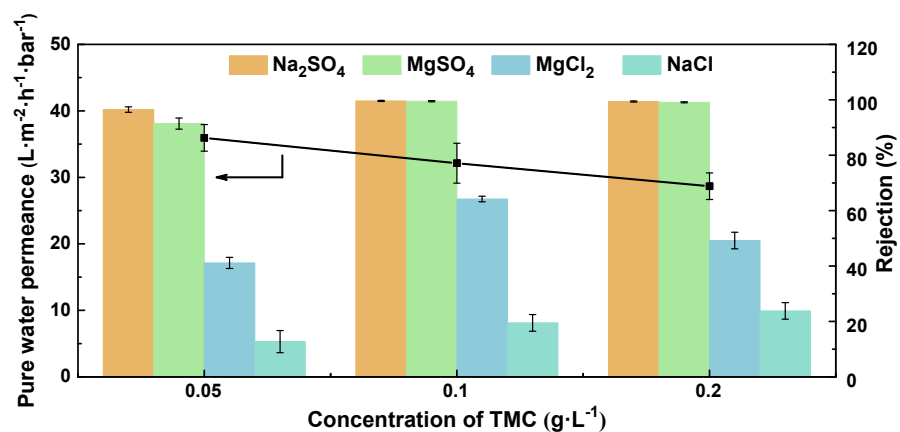
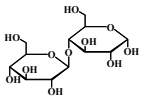
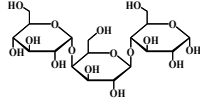
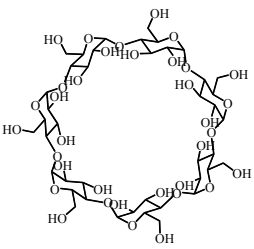


Fig. S24. Separation performance of the ULPA composite membranes prepared with different TMC concentrations. The ULPA nanofilms were prepared from 0.125 g L⁻¹ PIP and 0.050 g L⁻¹ GQDs at free aqueous-organic interface for 60 s with different TMC concentrations.

Table S3. Spherical neutral solutes with various molecular weights were selected for rejection tests.

Spherical solutes	Molecular structure	Molecular weight (Da)	Stokes radius (nm) ²	Rejection (%)	
				PA	ULPA-2
Isobutanol		74	0.279	16.6±3.0	16.2±2.8
Glucose		180	0.358	69.2±2.0	58.4±2.0
Sucrose		342	0.462	91.2±1.5	86.1±2.5
Raffinose		504	0.584	93.5±2.0	93.0±3.0
β-cyclodextrin		1134	0.742	94.7±3.0	93.3±2.0

The MWCO of ULPA composite membranes was determined by the rejection of 90% for spherical neutral solutes including isobutanol, glucose, sucrose, raffinose and β-cyclodextrin. The operating conditions were 100 ppm feed solution and stabilization for 0.5 h under 2.0 bar. The rejection of solutes was calculated based on the eqn 4 in the text, where the concentrations of the permeate and feed solution were detected by a total organic carbon (TOC) analyzer (Leichi, HTY-CT1000A, China). The mean pore size of composite membranes equals the Stokes radius of the spherical solute with a 50% rejection. The pore size distribution, expressed as a probability density function, is deduced by the following eqn S3:

$$\frac{dR(r_p)}{dr_p} = \frac{1}{r_p \ln \sigma_p \sqrt{2\pi}} \exp \left[-\frac{(\ln r_p - \ln \mu_p)^2}{2(\ln \sigma_p)^2} \right] \quad (\text{S3})$$

where μ_p is the mean pore size and is calculated by correlating the Stokes radius of spherical solutes, σ_p is equal to the ratio of the solute radius at $R_p=84.13\%$ to $R_p=50.00\%$, and r_p is the Stokes radius of the spherical solute.^{3,4}

Table S4. Pure water permeance of the ULPA composite membranes and ultrathin polyamide composite membranes.

Type	Nanofilm thickness (nm)	Pure water permeance (L m ⁻² h ⁻¹ bar ⁻¹)				Increment (L m ⁻² h ⁻¹ bar ⁻¹)
		Nanofilm		Composite membranes		
		ULPA	Ultrathin polyamide	ULPA	Ultrathin polyamide	
PA	18.3	12.8	12.8	12.4	12.4	0
ULPA-1	13.2	-	17.7	17.8	17.0	0.8
ULPA-2	10.5	-	22.3	32.1	21.1	11.0
ULPA-3	8.3	-	28.2	46.0	26.3	19.7
ULPA-4	5.5	-	42.3	65.8	38.2	27.6

Note: the pure water permeance of PAN substrate was 400 L m⁻² h⁻¹ bar⁻¹.

A simple resistances-in-series model was applied to describe water transport through the thin-film composite membranes consisting a polyamide nanofilm on a substrate.⁵ The permeance of composite membranes, $P_{\text{composite membranes}}$, should follow eqn S4. The permeance of polyamide nanofilms and substances, P_{nanofilm} and $P_{\text{substance}}$, also can be described by eqn S5, and S6, respectively.

$$P_{\text{composite membranes}} = \frac{1}{R_{\text{substance}} + R_{\text{nanofilm}}} \quad (\text{S4})$$

$$P_{\text{nanofilm}} = \frac{1}{R_{\text{nanofilm}}} \quad (\text{S5})$$

$$P_{\text{substance}} = \frac{1}{R_{\text{substance}}} \quad (\text{S6})$$

where R_{nanofilm} is the resistance of polyamide nanofilms, and $R_{\text{substance}}$ is the resistance of substances.

By substituting resistances of the polyamide nanofilms and the substances from eqn S4 and S6 into eqn S5, the permeance of polyamide nanofilms, P_{nanofilm} , can be obtained as:

$$P_{\text{nanofilm}} = \frac{1}{\frac{1}{P_{\text{composite membranes}}} - \frac{1}{P_{\text{substance}}}} \quad (\text{S7})$$

where $P_{\text{composite membranes}}$ and $P_{\text{substance}}$ can be obtained in the experiment.

In the text, the permeance of PA composite membranes and PAN substance were 12.4 and 400 L m⁻² h⁻¹ bar⁻¹, respectively. According to eqn S7, the permeance of PA nanofilm (P_{PA}) can be calculated as:

$$P_{PA} = \frac{1}{\frac{1}{P_{\text{composite membranes}}} - \frac{1}{P_{\text{substance}}}} = \frac{1}{\frac{1}{12.4} - \frac{1}{400}} = 12.8 \text{ L m}^{-2}\text{h}^{-1}\text{bar}^{-1} \quad (\text{S8})$$

As the usual assumption is that the permeance is inversely proportional to thickness, the pure water permeance of ultrathin polyamide nanofilm is obtained by the scaling of the permeance and thickness of PA nanofilm. Then, the resistance of a series of ultrathin polyamide nanofilms with corresponding thickness can be calculated from eqn S5 by the correlated permeance. The resistance of PAN substance can be calculated from eqn S6 by measuring the substance permeance as 400 L m⁻² h⁻¹ bar⁻¹. Finally, by substituting resistances of the nanofilm and the PAN substance from eqn S5 and S6 into eqn S4, the pure water permeance of ultrathin polyamide composite membranes can be obtained, as shown in Table S4.

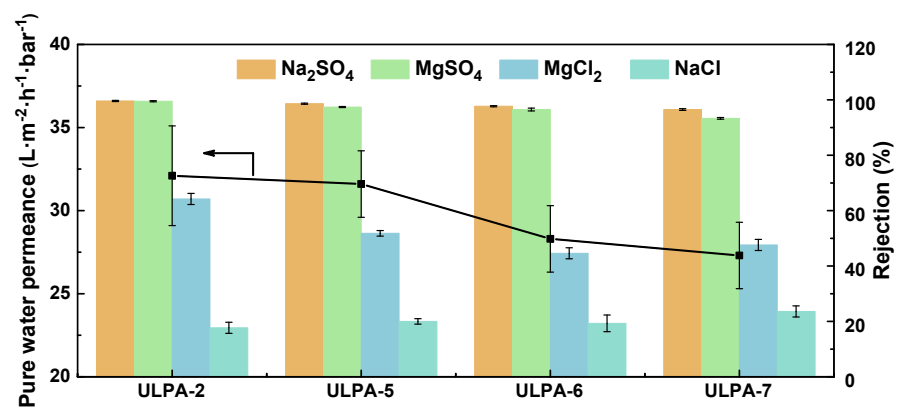


Fig. S25. Separation performance of the ULPA composite membranes prepared by LGQDs. ULPA-2) GQDs; ULPA-5) LGQDs-17; ULPA-6) LGQDs-45; ULPA-7) LGQDs-110.

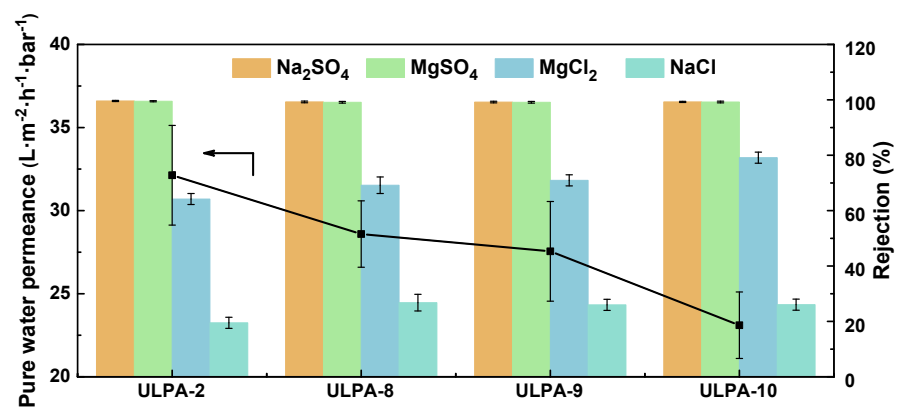


Fig. S26. Separation performance of the ULPA composite membranes prepared by RGQDs. ULPA-2) GQDs; ULPA-8) RGQDs-0.61; ULPA-9) RGQDs-0.60; ULPA-10) RGQDs-0.58.

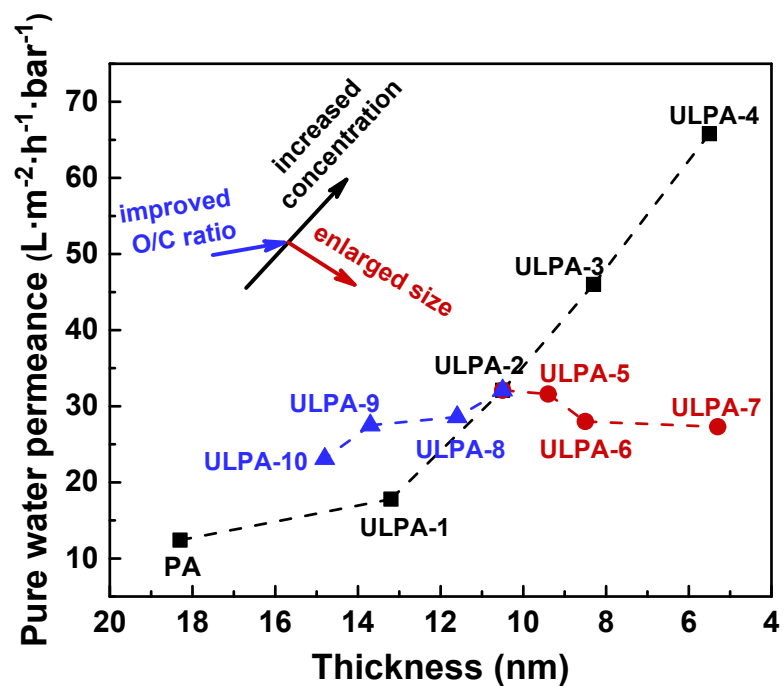


Fig. S27. Variation of pure water permeance of the ULPA composite membranes versus the nanofilm thickness. As expected, the ever-thinner ULPA nanofilms were achieved as increasing concentration, size or O/C ratio of GQDs. However, unlike increasing the concentration and O/C ratio of GQDs to reduce the thickness to elevate the permeance, increasing the size of GQDs makes the nanofilm thinner but actually decrease the permeance.

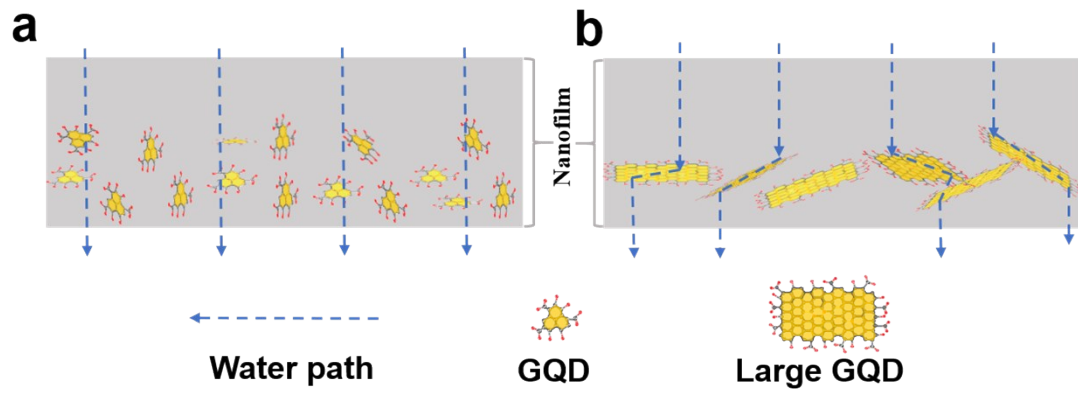


Fig. S28. Water molecules transport through ULPA nanofilms with GQDs (a) and large-diameter GQDs (b). The large-diameter GQDs result in a more tortuous travel path for water molecules than small ones.

Table S5. Water permeance and salt rejection of the ULPA composite membranes.

Membrane	Pure water permeance (L m ⁻² h ⁻¹ bar ⁻¹)	Na ₂ SO ₄		MgSO ₄		MgCl ₂		NaCl	
		Water permeance (L m ⁻² h ⁻¹ bar ⁻¹)	Rejection (%)	Water permeance (L m ⁻² h ⁻¹ bar ⁻¹)	Rejection (%)	Water permeance (L m ⁻² h ⁻¹ bar ⁻¹)	Rejection (%)	Water permeance (L m ⁻² h ⁻¹ bar ⁻¹)	Rejection (%)
PA	12.4±2.0	9.8±1.5	99.4±0.2	10±2.0	98.8±0.3	9.9±1.8	83.7±1.0	11.6±2.0	21.7±2.0
ULPA-1	17.8±3.0	15.1±2.5	99.5±0.1	15.5±2.8	99.5±0.2	16.2±2.8	79.0±1.5	16.2±2.5	17.7±1.5
ULPA-2	32.1±3.0	25.4±4.0	99.6±0.2	27.4±4.0	99.5±0.2	30.4±3.0	64.2±2.0	30.4±4.5	17.7±2.0
ULPA-3	46.0±3.0	37.4±3.5	98.5±0.5	38.2±2.5	95.6±1.0	44.8±2.5	39.1±0.8	45.4±3.5	17.1±2.0
ULPA-4	65.8±3.0	43.0±3.0	93.7±1.2	51.6±3.5	87.7±1.5	61.2±3.5	35.5±2.0	64.1±3.5	12.1±1.6

Table S6. Performance comparison of various membranes in Cl⁻/SO₄²⁻ selectivity.

Membrane	Pure water permeance (L·m ⁻² ·h ⁻¹ ·bar ⁻¹)	Rejection (%)		Cl ⁻ /SO ₄ ²⁻ selectivity, S	Testing conditions	Ref.
		Na ₂ SO ₄	NaCl			
TS-II	26.04	99.6	49.6	126.0	2000 ppm, 4.8 bar, cross-flow	6
PA/PD/ZIF-8/SWCNTs	53.5	95	11	17.8	1000 ppm, 4.0 bar, cross-flow	7
PA/PD/SWCNTs	32	95.9	23	18.8	1000 ppm, 6.0 bar, cross-flow	8
PA/SWCNTs	40	96.5	13.4	24.7	1000 ppm, 6.0 bar, cross-flow	9
NCM	25.1	99.1	27.5	80.6	1500 ppm, 4.0 bar, cross-flow	10
ZNGTFNMs	10.63	97.8	31.6	31.1	1000 ppm, 6.0 bar, cross-flow	11
PIP/Sericin-TMC NF2	16.4	97.3	32	25.2	500 ppm, 5.0 bar, cross-flow	12
TFC2.0.5	14.5	97	27.7	24.1	1000 ppm, 4.0 bar, cross-flow	13
TFN-mZIF2	14.9	93	11.5	12.6	1000 ppm, 4.0 bar, cross-flow	14
PA-PPTA/PSf 8	8.52	99.1	63.6	40.44	1000 ppm, 5.0 bar, cross-flow	15
NFM-3	5.6	98.8	35	54.17	1000 ppm, 4.0 bar, cross-flow	16
M _{2-C}	13.6	94.2	23	13.3	500 ppm, 2.0 bar, cross-flow	17
THPC-5	50.5	98.4	23.2	48.0	1000 ppm, 6.0 bar, cross-flow	18
TFC-PA (SARIP)	17.1	99.6	27	128.5	1000 ppm, 4.0 bar, cross-flow	4
PA	12.4	99.4	21.7	130.5	1000 ppm, 2.0 bar, cross-flow	
ULPA-1	17.8	99.5	17.7	164.6	1000 ppm, 2.0 bar, cross-flow	
ULPA-2	32.1	99.6	17.7	205.8	1000 ppm, 2.0 bar, cross-flow	This work
ULPA-8	28.6	99.3	26.8	104.6	1000 ppm, 2.0 bar, cross-flow	
ULPA-9	27.6	99.2	26	92.5	1000 ppm, 2.0 bar, cross-flow	
ULPA-10	23.1	99.3	26	105.7	1000 ppm, 2.0 bar, cross-flow	

Table S7. Separation performance of the ULPA composite membranes for mixed feed containing 500 ppm NaCl and 500 ppm Na₂SO₄.

Sample	Cl ⁻ (mg L ⁻¹)	SO ₄ ²⁻ (mg L ⁻¹)	R (Cl ⁻)	R (SO ₄ ²⁻)	Cl ⁻ /SO ₄ ²⁻ selectivity, S _m
Feed	319.8	360.0	--	--	--
PA	285.7	1.2	10.66	99.67	270.7
ULPA-1	290.1	0.8	9.29	99.78	412.3
Permeate ULPA-2	293.8	0.5	8.13	99.86	656.2
ULPA-3	299.7	4.5	6.29	98.75	75.0
ULPA-4	319.7	13.7	0.03	96.19	26.2

Solution-diffusion model

The transport of water and salt through polyamide nanofilms can be described by the solution-diffusion model.¹⁹ The water flux across nanofilm is calculated by the following eqn S9:

$$J_w = A(\Delta p - \Delta \pi) \quad (S9)$$

where J_w is the water flux ($L m^{-2} h^{-1}$), A ($L m^{-2} h^{-1} bar^{-1}$), Δp (bar) and $\Delta \pi$ (bar) are the water permeability constant, the applied hydrostatic pressure and the osmotic pressure difference across the nanofilm, respectively. Like the water flux, the salt flux through nanofilm is given by the following eqn S10:

$$J_s = B \Delta c_s \quad (S10)$$

where J_s is the salt flux ($mg m^{-2} h^{-1}$), B is the salt permeability constant ($m h^{-1}$), and Δc_s is the salt concentration difference ($\Delta c_s = c_f - c_p$). Δc_s and $\Delta \pi$ have the following relationship:

$$\Delta \pi = \Delta c_s RT \quad (S11)$$

The constant A is related to water permeability as following:

$$A = \frac{P_w}{L} \frac{M_w}{RT} \quad (S12)$$

where P_w is the water permeability ($cm^2 s^{-1}$), M_w ($g mol^{-1}$), L (cm), R ($83.1 cm^3 \cdot bar mol^{-1} \cdot K^{-1}$) and T (K) are the molecular weight of water, the thickness of nanofilm, the gas constant and the absolute temperature, respectively. The salt permeability is defined as following eqn S13:

$$B = \frac{P_s}{L} \quad (S13)$$

where P_s is the salt permeability ($cm^2 s^{-1}$). According to the solution-diffusion mechanism, the water-salt selectivity, $\alpha_{w/s}$ is defined as the ratio of water permeability to salt permeability:

$$\alpha_{w/s} = \frac{P_w}{P_s} \quad (S14)$$

The selectivity is a material property describing the ability of a nanofilm to separation water and salts. The trade-off and upper-bound relationship between the water permeability and water-salt selectivity is:

$$\frac{P_w}{P_s} = \frac{\lambda}{(P_w)^\beta} \quad (S15)$$

where λ and β are empirical fitting parameters. For the permselectivity trade-off relationship of the nanofilms, $\lambda=0.37 \times 10^{-7} \text{ cm}^4 \text{ s}^{-2}$ and $\beta=2$. For the upper-bound relationship, $\lambda=1.4 \times 10^{-7} \text{ cm}^4 \text{ s}^{-2}$ and $\beta=2$.⁶

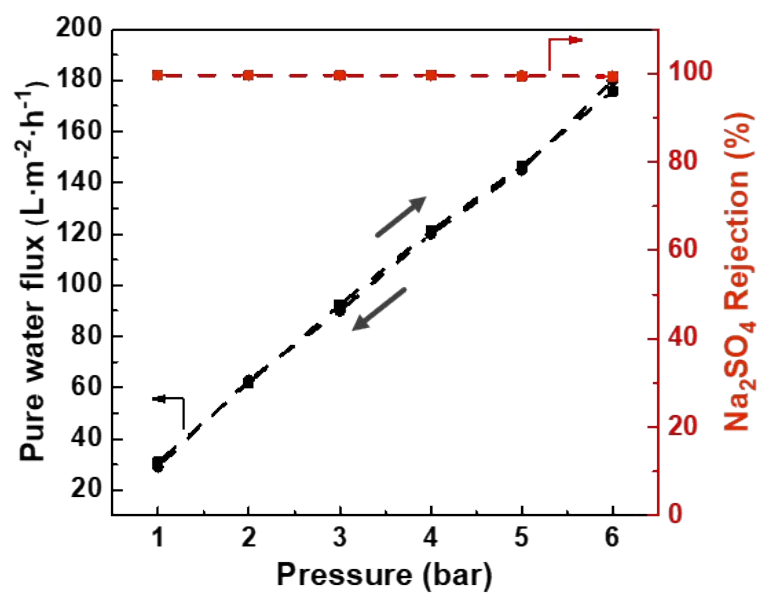


Fig. S29. The separation performance of the UPLA-2 composite membranes at 1000 ppm Na₂SO₄ in pressure cycling experiment.

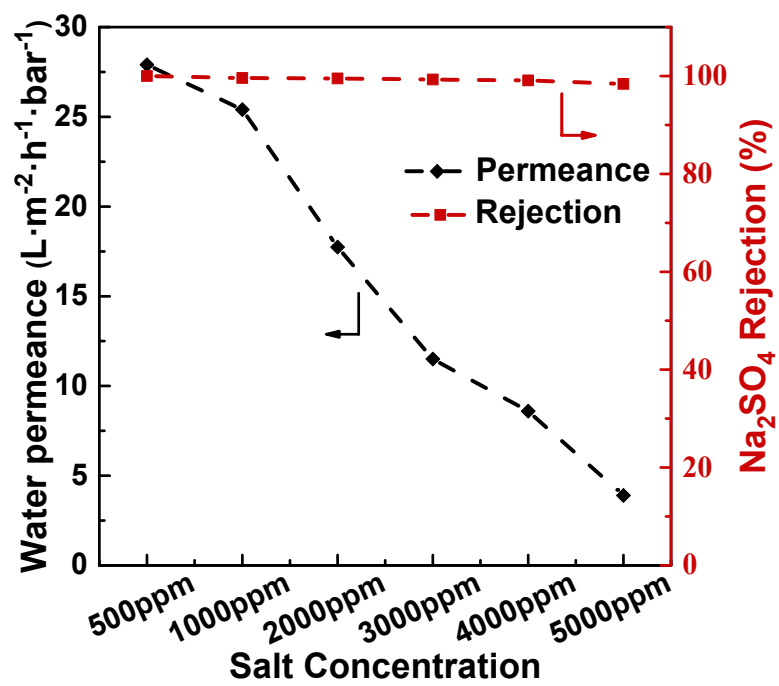


Fig. S30. Water permeance and rejection of the ULPA-2 composite membranes under different Na₂SO₄ concentrations.

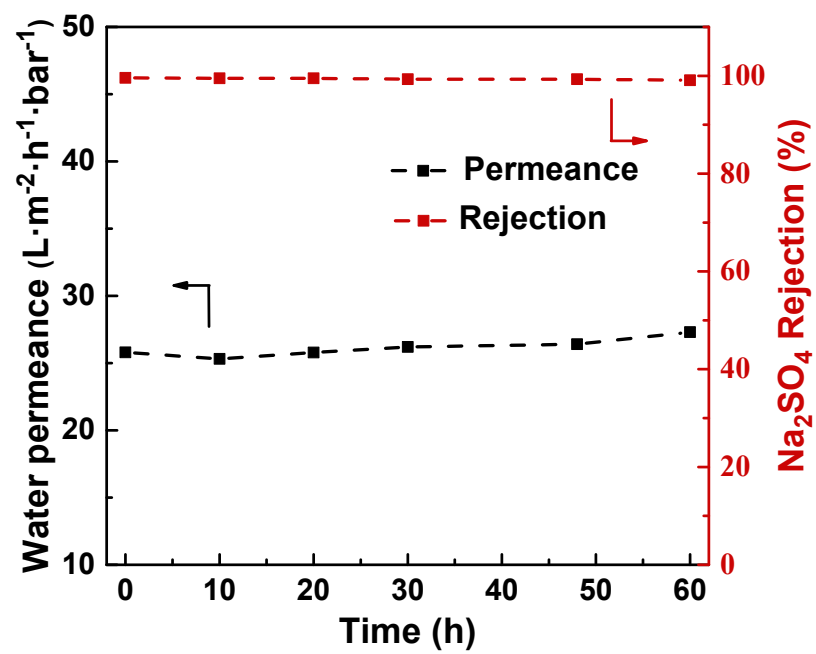


Fig. S31. Stability of the ULPA-2 composite membranes in HCl solution (pH=1).

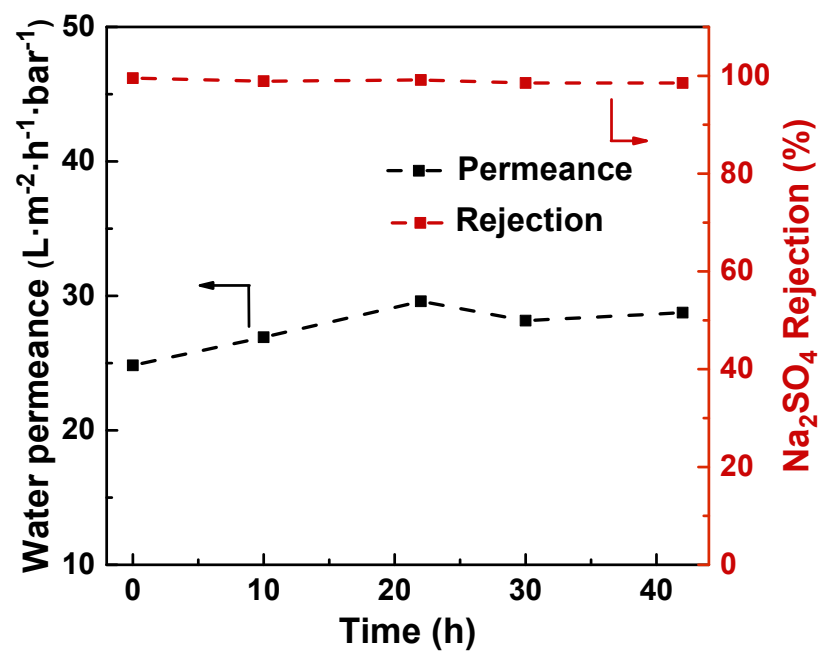


Fig. S32. Chlorine resistance property of the ULPA-2 composite membranes as immersing membranes in 1000 ppm NaClO solution.

References

- 1 X. You, T. Ma, Y. Su, H. Wu, M. Wu, H. Cai, G. Sun and Z. Jiang, *Journal of Membrane Science*, 2017, **540**, 454-463.
- 2 S. P. Sun, T. A. Hatton and T. Chung, *Environmental Science & Technology*, 2011, **45**, 4003-4009.
- 3 J. Gao, S. Sun, W. Zhu and T. Chung, *Journal of Membrane Science*, 2014, **452**, 300-310.
- 4 Y. Liang, Y. Zhu, C. Liu, K. Lee, W. Hung, Z. Wang, Y. Li, M. Elimelech, J. Jin and S. Lin, *Nature Communications*, 2020, **11**, 2015.
- 5 Z. Jiang, S. Karan and A. G. Livingston, *Advanced Materials*, 2018, **30**, 1705973.
- 6 Z. Tan, S. Chen, X. Peng, L. Zhang and C. Gao, *Science*, 2018, **360**, 518-521.
- 7 Z. Wang, Z. Wang, S. Lin, H. Jin, S. Gao, Y. Zhu and J. Jin, *Nature Communications*, 2018, **9**, 2004.
- 8 Y. Zhu, W. Xie, S. Gao, F. Zhang, W. Zhang, Z. Liu and J. Jin, *Small*, 2016, **12**, 5034-5041.
- 9 S. Gao, Y. Zhu, Y. Gong, Z. Wang, W. Fang and J. Jin, *ACS Nano*, 2019, **13**, 5278-5290.
- 10 J. Zhu, J. Hou, R. Zhang, S. Yuan, J. Li, M. Tian, P. Wang, Y. Zhang, A. Volodin and B. Van der Bruggen, *Journal of Materials Chemistry A*, 2018, **6**, 15701-15709.
- 11 Y. Ji, Q. An, X. Weng, W. Hung, K. Lee and C. Gao, *Journal of Membrane Science*, 2018, **548**, 559-571.
- 12 Y. Pan, R. Xu, Z. Lu, S. Yu, M. Liu and C. Gao, *Journal of Membrane Science*, 2017, **523**, 282-290.
- 13 J. Zhu, S. Yuan, A. Uliana, J. Hou, J. Li, X. Li, M. Tian, Y. Chen, A. Volodin and B. Van der Bruggen, *Journal of Membrane Science*, 2018, **554**, 97-108.
- 14 J. Zhu, L. Qin, A. Uliana, J. Hou, J. Wang, Y. Zhang, X. Li, S. Yuan, J. Li, M. Tian, J. Lin and B. Van der Bruggen, *ACS Applied Materials & Interfaces*, 2017, **9**, 1975-1986.
- 15 Q. Shi, L. Ni, Y. Zhang, X. Feng, Q. Chang and J. Meng, *Journal of Materials Chemistry A*, 2017, **5**, 13610-13624.
- 16 J. Wang, Y. Wang, J. Zhu, Y. Zhang, J. Liu and B. Van der Bruggen, *Journal of Membrane Science*, 2017, **533**, 279-288.
- 17 T. Wang, H. Qiblawey, S. Judd, A. Benamor, M. S. Nasser and A. Mohammadian, *Journal of Membrane Science*, 2018, **552**, 222-233.
- 18 H. Peng, W. Zhang, W. Hung, N. Wang, J. Sun, K. Lee, Q. An, C. Liu and Q. Zhao, *Advanced Materials*, 2020, **32**, 2001383.
- 19 G. M. Geise, H. B. Park, A. C. Sagle, B. D. Freeman and J. E. McGrath, *Journal of Membrane Science*, 2011, **369**, 130-138.